Theoretical simulation of electroacoustic borehole logging in a fluid-saturated porous formation

Hengshan Hu[a] and Wei Guan
Department of Astronautics and Mechanics, Harbin Institute of Technology, Postbox 344, 92 West Dazhi Street, Harbin, 150001, China

Jerry M. Harris
Department of Geophysics, Stanford University, Stanford, California 94305

(Received 13 September 2006; revised 29 March 2007; accepted 9 April 2007)

Electroacoustic (E-A) logging describes the acoustic response to an electromagnetic (EM) source in a fluid-filled borehole surrounded by a porous medium. The E-A response is simulated by two different methods in this paper. In the coupled method, the EM field and the acoustic field are modeled using Pride's model, which couples Maxwell's equations and Biot's equations. In the uncoupled method, the EM field is uninfluenced by the converted acoustic field, resulting in separate acoustic formulation with an electrokinetic source term derived from the primary EM field. The difference of the transient full waveforms between the above two methods is remarkably small for all examples, thus confirming the validity of using the computationally simpler uncoupled method. It is shown from the simulated waveforms that an EM-accompanying acoustic field is coupled to the EM field and appears with an apparent phase velocity of the EM wave in the formation. Acoustic waves with the conventional acoustic velocities are also seen in the converted full waveforms. For the sandstone models used in this paper, when permeability is less than 1 Darcy, the E-A Stoneley wave amplitude increases with porosity, which is different from that in conventional acoustic-to-acoustic logging.
 [DOI: 10.1121/1.2735809]

PACS number(s): 43.30.Ky, 43.20.Bi, 43.40.Ph [RAS] Pages: 135–145

I. INTRODUCTION

In a fluid-saturated porous medium, acoustic (or seismic) and electromagnetic (EM) waves are coupled because of electrokinetic effect. The electrokinetic effect is related to the electric double layer (EDL) at the solid-fluid interface (Pride and Morgan, 1991) and the flow of pore fluid relative to the porous solid matrix. When an acoustic wave propagates through a fluid-saturated porous medium, relative fluid flow occurs (Biot, 1956, 1962), which in turn carries excess ions in the EDL, causing convection electric current and a streaming potential. This phenomenon is called acoustoelectric (A-E) conversion. Reversely, when an EM wave propagates, the electric field exerts forces on the ions in the EDL, which causes the relative flow between the fluid and the solid phases, producing pressure gradients and an acoustic wave. This phenomenon is known as electroacoustic (E-A) conversion.

Ivanov (1940) measured the electric signal caused by the electrokinetic effect. In order to explain the phenomenon observed by Ivanov, Frenkel (1944) established a theoretical model of poro-acoustics and attempted to study the relation between the relative flow induced by a seismic wave and the flow-induced electric field. He predicted that an electric field accompanies a compressional seismic wave in homogeneous porous medium. Nevertheless, he did not allow for the full set of Maxwell's equations so that he mistakenly concluded that shear waves do not induce EM disturbances. In the following 50 years, many experimental observations were conducted (such as Martner and Sparks, 1959; Broding *et al.*, 1963; and Long and Rivers, 1975), but few theoretical developments (e.g., Neev and Yeatts, 1989) were reported.

Substantial developments were achieved since the 1990s, due to fast development in signal recording and processing techniques and due to ever-increasing demand for earth resources. Pride (1994) derived from first principles the governing equations for coupled acoustic and EM fields in homogeneous porous media, which is a combination of Biot's equations of poroelasticity (Biot, 1956, 1962) and Maxwell's equations of electromagnetism. Pride and Haartsen (1996) obtained expressions for electroseismic plane waves in a homogeneous porous medium. Haartsen and Pride (1997) presented the numerical simulations of the seismoelectric fields excited by an acoustic point-source in the fluid-saturated stratified porous medium. There are two kinds of fields shown to exist: one is the stationary electric and magnetic fields accompanying seismic waves during their propagation, with no extent outside of the seismic pulses; the other is the independently propagating EM wave generated by seismic waves when traveling across medium interfaces. These important publications provided a theoretical framework to interpret the experimental observations. Along with the developments of theoretical studies, many field and laboratory studies as well as numerical simulations were reported. Thompson and Gist (1993), Butler *et al.* (1996), and Mikhailov *et al.* (1997), implemented the field studies about

[a]Electronic mail: wave_hu@yahoo.com

electrokinetic effect and demonstrated the above-mentioned two kinds of EM fields induced by a seismic source. While their studies revealed the potential use of wave-related electrokinetic effects in mapping subsurface fluid flow and in obtaining other useful information about the subsurface, the exploration depth is limited by the weak electric signals, resulting from the propagation attenuation from the source to the exploration target and back to the receivers on the ground surface. A-E logging and E-A logging were brought forward in the 1990s, which have much smaller source to target and target to receiver distances so that the exploration depth is not limited. Both the source and receiver are located in the borehole, and the formation to be measured is in the depth interval between the receiver and transmitter. In a series of publications, Zhu *et al.* (1999) and Zhu and Toksöz (2003, 2005) measured the induced EM signals of A-E logging by the use of scaled model wells in the laboratory. Hu (2000) and Hu and Liu (2002) numerically simulated the axisymmetric fields of A-E logging in a homogeneous fluid-saturated porous medium based on Pride's theory, and both the stationary and propagating EM fields were seen in their simulated waveforms.

Most of the above-mentioned studies are concerned with A-E conversion of the electrokinetic effect. Zhu *et al.* (1999) recorded distinct E-A Stoneley waves induced by an electrode in his scaled model wells. His experimental result showed the possibility of a new borehole logging technique that could explore more physical properties related to the fluid and its flow in the porous formations. Recently Thompson (2005) and Thompson *et al.* (2005) reported field experiments about E-A conversion. They summarized the results of E-A field tests in three locations and concluded that E-A conversion is a sensitive indicator of hydrocarbon saturation, which revealed potential applications of E-A conversion. Nevertheless, we have not seen published theoretical papers on E-A logging.

In this paper we simulate the acoustic field excited by a vertical electric dipole in the borehole due to electrokinetic effect in the porous formation. The major objective is to derive the E-A wave fields analytically and analyze the full waveforms. The paper is organized as below. In Sec. II, we provide two different methods for simulating E-A logging. In the first three subsections the acoustic field and EM field in the formation are seen as coupled and are formulated based on Pride's equations and boundary conditions. In the last subsection, the EM field is formulated separately by ignoring the influence of the electrokinetically induced acoustic field on the EM field itself, and the acoustic field is then formulated by taking the EM disturbances as a source term. In Sec. III, we calculate the acoustic as well as the electric waveforms for typical logging situations using expressions derived in Sec. II. Transient full waveforms are obtained by the above two methods and are compared. We continue to analyze the interrelationships between the waveforms and the porosity and permeability of the formation.

II. FORMULATION

A. Fields in the porous formation

The governing equations that describe the coupling between the acoustic and electric fields in homogeneous fluid-saturated porous medium were derived by Pride (1994) and can be expressed as follows, assuming $e^{-i\omega t}$ time dependence of all fields:

$$\nabla \times \mathbf{E} = i\omega \mathbf{B}, \tag{1}$$

$$\nabla \times \mathbf{H} = -i\omega \mathbf{D} + \mathbf{J}, \tag{2}$$

$$\mathbf{B} = \mu \mathbf{H}, \tag{3}$$

$$\mathbf{D} = \varepsilon \mathbf{E}, \tag{4}$$

$$\mathbf{J} = \sigma \mathbf{E} + L(-\nabla p + \omega^2 \rho_f \mathbf{u}), \tag{5}$$

$$-i\omega \mathbf{w} = L\mathbf{E} + (-\nabla p + \omega^2 \rho_f \mathbf{u})\kappa/\eta, \tag{6}$$

$$\boldsymbol{\nabla} \cdot \boldsymbol{\tau} = -\omega^2(\rho \mathbf{u} + \rho_f \mathbf{w}), \tag{7}$$

$$\boldsymbol{\tau} = (H - 2G)(\nabla \cdot \mathbf{u})\mathbf{I} + C(\nabla \cdot \mathbf{w})\mathbf{I} + G(\nabla \mathbf{u} + \nabla \mathbf{u}^{\mathbf{T}}), \tag{8}$$

$$-p = C\nabla \cdot \mathbf{u} + M\nabla \cdot \mathbf{w}, \tag{9}$$

where **E**, **D**, **J**, **B**, and **H** are the electric field, electric flux density, electric current density, magnetic flux density, and magnetic field, respectively, **u** is the displacement of the solid phase, **w** is the relative flow between the fluid and the solid phase, $\boldsymbol{\tau}$ is the bulk stress tensor, **I** is the identity tensor, p is the pore fluid pressure, ε is the permittivity of the formation, μ is the magnetic permeability of the formation and is assumed to equal to that of vacuum in this paper, ρ_f and η are density and viscosity of the pore fluid, respectively, ρ is the density of the formation, G is the shear modulus of the formation, H, C, and M are porous-medium moduli as defined by Biot (1962), κ is the dynamic permeability defined by Johnson *et al.* (1987), σ and L are the conductivity and electrokinetic coupling coefficient of the formation, respectively. Expressions for σ and L used in our calculation can be found in the paper by Pride (1994). In the low frequency limit, the expression for L is given by

$$L = -\frac{\phi}{\alpha_\infty}\frac{\varepsilon_f \varsigma}{\eta}\left(1 - 2\alpha_\infty \frac{\tilde{d}}{\Lambda}\right), \tag{10}$$

where ε_f is the permittivity of the fluid in the porous formation; α_∞ is the tortuosity; ς is called the zeta potential, which is the electric potential at the shear plane, the surface that separates the two layers, i.e., the adsorbed layer and the diffuse layer in the EDL; and Λ and $\tilde{d}$ are the weighted volume-to-surface radio and a length that is equal to or less than the Debye length, respectively, defined by Pride (1994). Electrokinetic coupling between acoustic fields and EM fields is reflected in Eqs. (5) and (6) through the terms with the coefficient L. If L is set to zero, the two equations decouple into Biot's and Maxwell's equations. The coefficient L is proportional to porosity in the low frequency limit [see Eq. (10)]

and is approximately proportional to porosity at higher frequencies.

In E-A logging the source is located in the borehole so that there are neither acoustic nor EM sources in the fluid-saturated porous formation. From Eqs. (1)–(9) one can derive equations in terms of **u**, **w**, and **E** as below:

$$(H-G)\nabla\nabla\cdot\mathbf{u}+G\nabla^2\mathbf{u}+\omega^2\rho\mathbf{u}+C\nabla\nabla\cdot\mathbf{w}+\omega^2\rho_f\mathbf{w}=0, \tag{11}$$

$$C\nabla\nabla\cdot\mathbf{u}+\omega^2\rho_f\mathbf{u}+M\nabla\nabla\cdot\mathbf{w}+\omega^2\bar{\rho}\mathbf{w}-i\omega\bar{\rho}L\mathbf{E}=0, \tag{12}$$

$$\nabla\nabla\cdot\mathbf{E}-\nabla^2\mathbf{E}-\omega^2\mu\bar{\varepsilon}\mathbf{E}+i\omega^3\mu\bar{\rho}L\mathbf{w}=0, \tag{13}$$

where

$$\bar{\varepsilon}=\varepsilon+i\sigma/\omega-\bar{\rho}L^2 \tag{14}$$

is the effective complex permittivity of the formation, and

$$\bar{\rho}=i\eta/(\omega\cdot\kappa) \tag{15}$$

is the effective density for relative flow.

According to the Helmholtz theorem, the fields **u**, **w**, and **E** in Eqs. (11)–(13) can be expressed in terms of potential functions. It can be shown through complex mathematical operations as in the paper by Pride and Haartsen (1996) that there are four different modes of waves in an infinite homogeneous fluid-saturated porous medium. Two of them are rotation-free waves, i.e., the fast compressional wave whose wave number is k_{pf}, and the slow compressional wave whose velocity is k_{ps}. The other two are divergence-free waves, i.e., the shear wave whose wave number is k_{sh}, and the EM wave whose wave number is k_{em}. The fields **u**, **w**, and **E** are coupled due to electrokinetic effect, and each of them can travel with the above four different wave numbers. The amplitudes and phases of the three fields are different. For example, **u**, **w**, and **E** can all travel with the fast compressional wave number, with $\mathbf{w}_{pf}=\alpha_{pf}\mathbf{u}_{pf}$ and $\mathbf{E}_{pf}=\beta_{pf}\mathbf{u}_{pf}$. The amplitude ratio and phase shift are reflected by α_{pf} between $\mathbf{w}_{pf}$ and $\mathbf{u}_{pf}$, and by β_{pf} between $\mathbf{E}_{pf}$ and $\mathbf{u}_{pf}$. The expressions for the wave numbers k_i and the factors α_i, β_i ($i=pf,ps,sh,em$) are given by Pride and Haartsen (1996) and Hu (2000).

Let us study the axisymmetric fields excited by a vertical electric dipole along the borehole axis. We adopt the cylindrical coordinate system (r, z, θ), with the z axis being the borehole axis, and the origin coinciding with the center of the dipole. In the porous formation the TM wave (the transverse magnetic wave, i.e., the magnetic field is perpendicular to the $r-z$ plane and the electric field is in the $r-z$ plane) is coupled with the P wave and the SV wave (the shear wave whose motion is in the $r-z$ plane) due to the electrokinetic effect. As a result, an axisymmetric EM field is associated with an axisymmetric acoustic field. From the above analysis, we can express **u**, **w**, and **E** by potential functions as below:

$$\mathbf{u}=A_{pf}\nabla\phi_{pf}+A_{ps}\nabla\phi_{ps}+A_{sh}\nabla\times(\Gamma_{sh}\mathbf{e}_\theta)+A_{em}\nabla\times(\Gamma_{em}\mathbf{e}_\theta), \tag{16}$$

$$\mathbf{w}=\alpha_{pf}A_{pf}\nabla\phi_{pf}+\alpha_{ps}A_{ps}\nabla\phi_{ps}+\alpha_{sh}A_{sh}\nabla\times(\Gamma_{sh}\mathbf{e}_\theta)+\alpha_{em}A_{em}\nabla\times(\Gamma_{sh}\mathbf{e}_\theta), \tag{17}$$

$$\mathbf{E}=\beta_{pf}A_{pf}\nabla\phi_{pf}+\beta_{ps}A_{ps}\nabla\phi_{ps}+\beta_{sh}A_{sh}\nabla\times(\Gamma_{sh}\mathbf{e}_\theta)+\beta_{em}A_{em}\nabla\times(\Gamma_{sh}\mathbf{e}_\theta), \tag{18}$$

where the potentials are

$$\phi_m=K_0(\eta_m r)e^{ikz}\quad(m=pf,ps), \tag{19}$$

$$\Gamma_n=K_1(\eta_n r)e^{ikz}\quad(n=sh,em), \tag{20}$$

where k is the axial wave number, η_m and η_n are the radial wave numbers, i.e., $\eta_m=\sqrt{k^2-k_m^2}$ and $\eta_n=\sqrt{k^2-k_n^2}$, I_n and K_n are modified Bessel functions of the nth order. The coefficients A_i ($i=pf,ps,sh,em$) can be determined by the boundary conditions on the wall, and $\mathbf{e}_\theta$ is the unit vector in the θ direction.

Once **u**, **w**, and **E** are known, one can obtain the stress $\boldsymbol{\tau}$ and the E-A pressure p from Eqs. (8) and (9). The magnetic field **H** can be derived from Faraday's law

$$\mathbf{H}=\frac{1}{i\omega\mu}\nabla\times\mathbf{E}. \tag{21}$$

B. Fields in the borehole fluid

To simplify our simulation, we use an oscillating electric dipole as the source in E-A logging. It may be a short line conductor in which an alternating current flows. We assume the length l of the conductor is very short compared with the wavelength ($l\ll\lambda$) and the amplitude I_0 of the current is uniform along the entire length l. Assuming $e^{-i\omega t}$ time dependence, the radiation field of the dipole can be represented by a magnetic vector potential **A** as (Guru and Hiziroğlu, 2004)

$$\mathbf{A}=\mathbf{e}_z\frac{\mu_b p_e}{4\pi}\frac{1}{R}e^{ik_{be}R}, \tag{22}$$

where **A** is related to the magnetic flux density **B** and the electric field **E** by

$$\mathbf{B}=\nabla\times\mathbf{A}, \tag{23}$$

$$\mathbf{E}=i\omega\left(\mathbf{A}+\frac{1}{k_{be}^2}\nabla\nabla\cdot\mathbf{A}\right), \tag{24}$$

where μ_b is the magnetic permeability of the borehole fluid, and is assumed to equal to the magnetic permeability of vacuum, so we rewrite μ_b as μ in what follows, $R=\sqrt{r^2+z^2}$, $p_e=I_0 l$, $\mathbf{e}_z$ is the unit vector in the z direction and where

$$k_{be}^2=\omega^2\mu\varepsilon_b+i\omega\mu\sigma_b, \tag{25}$$

k_{be} is the EM wave number of the borehole fluid, ε_b and σ_b are dielectric constant and conductivity of the borehole fluid, respectively.

According to the theory of Bessel functions, $(1/R)e^{ik_{be}R}$ can be represented as

$$\frac{1}{R}e^{ik_{be}R} = \frac{1}{\pi}\int_{-\infty}^{\infty} K_0(\eta_{be}r)e^{ikz}\,dk, \tag{26}$$

where $\eta_{be}=\sqrt{k^2-k_{be}^2}$. So we have

$$\mathbf{A} = \mathbf{e}_z\frac{\mu p_e}{4\pi^2}\int_{-\infty}^{\infty} K_0(\eta_{be}r)e^{ikz}\,dk. \tag{27}$$

Substituting Eq. (27) into Eq. (23) and using the constitutive laws, i.e., Eq. (3), we can get the solution for the magnetic field, of which the only nonzero component is

$$H_\theta^R = \frac{p_e}{4\pi^2}\int_{-\infty}^{\infty} \eta_{be}K_1(\eta_{be}r)e^{ikz}\,dk, \tag{28}$$

where the superscript "R" represents the radiation field. Similarly, substituting Eq. (27) into Eq. (24), we get the solutions for the electric field,

$$E_r^R = \frac{\mu p_e}{4\pi^2}\int_{-\infty}^{\infty} \omega\frac{k\eta_{be}}{k_{be}^2}K_1(\eta_{be}r)e^{ikz}\,dk, \tag{29}$$

$$E_z^R = \frac{\mu p_e}{4\pi^2}\int_{-\infty}^{\infty} i\omega\left(1-\frac{k^2}{k_{be}^2}\right)K_0(\eta_{be}r)e^{ikz}\,dk, \tag{30}$$

with the θ component of the electric field being zero.

The solution for the total EM field in the borehole is composed of the particular solution, which represents the radiation field from the dipole, i.e., Eqs. (28)–(30), and the solution of the associated homogeneous equations, which represents a source-free field that obeys the Helmholtz equation,

$$\nabla^2\mathbf{E} + k_{be}^2\mathbf{E} = 0. \tag{31}$$

Using the fact that the divergence of the electric field vanishes in the source-free region, the solution of Eq. (31) can be expressed as

$$E_r^O = \int_{-\infty}^{\infty} B_e(k,\omega)I_1(\eta_{be}r)e^{ikz}\,dk, \tag{32}$$

$$E_z^O = -\int_{-\infty}^{\infty} \frac{\eta_{be}B_e}{ik}I_0(\eta_{be}r)e^{ikz}\,dk, \tag{33}$$

where the superscript "O" represents the source-free field. The θ component of the electric field is zero because of axisymmetry. From Eq. (21) we can get the magnetic field, of which the only nonzero component is

$$H_\theta^O = \frac{1}{\omega\mu}\int_{-\infty}^{\infty}\left(k-\frac{\eta_{be}^2}{k}\right)B_eI_1(\eta_{be}r)e^{ikz}\,dk. \tag{34}$$

The total EM field in the borehole can be obtained by adding together the above particular solution and the solution to the homogenous equation, i.e.,

$$E_r = E_r^R + E_r^O, \quad E_z = E_z^R + E_z^O, \quad H_\theta = H_\theta^R + H_\theta^O. \tag{35}$$

The acoustic field is not coupled with the EM field in the borehole. It exists due to the boundary condition requirements at the borehole wall. The displacement and pressure in the borehole can be represented by a scalar potential ϕ_{bm} as

$$\mathbf{u} = \nabla\phi_{bm}, \tag{36}$$

$$p = \rho_b\omega^2\phi_{bm}, \tag{37}$$

where ρ_b is the density of the borehole fluid, and ϕ_{bm} obeys the homogeneous Helmholtz equation,

$$\nabla^2\phi_{bm} + k_{bm}^2\phi_{bm} = 0, \tag{38}$$

where

$$k_{bm} = \frac{\omega}{V_{bm}}\left(1+\frac{i}{2Q_{bm}}\right) \tag{39}$$

is the acoustic wave number of the borehole fluid, and V_{bm} and Q_{bm} are the acoustic velocity and quality factor in the borehole fluid, respectively. The solution of Eq. (38) in the frequency domain can be expressed as

$$\phi_{bm}(r,z,\omega) = \frac{1}{\pi}\int_{-\infty}^{\infty} A_m(k,\omega)I_0(\eta_{bm}r)e^{ikz}\,dk, \tag{40}$$

where $\eta_{bm}=\sqrt{k^2-k_{bm}^2}$. Substituting Eq. (40) into Eqs. (36) and (37), one obtains

$$p = \frac{\rho_b\omega^2}{\pi}\int_{-\infty}^{\infty} A_m(k,\omega)I_0(\eta_{bm}r)e^{ikz}\,dk, \tag{41}$$

$$u_r = \frac{1}{\pi}\int_{-\infty}^{\infty} A_m(k,\omega)\,\eta_m I_1(\eta_{bm}r)e^{ikz}\,dk, \tag{42}$$

$$u_z = \frac{1}{\pi}\int_{-\infty}^{\infty} A_m(k,\omega)I_0(\eta_{bm}r)ike^{ikz}\,dk. \tag{43}$$

C. Boundary conditions

The coefficients A_i $(i=pf,ps,sh,em)$ in Eqs. (16)–(18), B_e in Eqs. (32)–(34), and A_m in Eqs. (40)–(43) can be determined from the following boundary conditions at the borehole wall:

$$u_{r0} = u_{r1} + w_{r1}, \tag{44}$$

$$p_0 = p_1, \tag{45}$$

$$-p_0 = \tau_{rr1}, \tag{46}$$

$$0 = \tau_{rz1}, \tag{47}$$

$$E_{z0} = E_{z1}, \tag{48}$$

$$H_{\theta0} = H_{\theta1}, \tag{49}$$

where quantities with subscript "0" are fields in the borehole, and quantities with subscript "1" are fields in the formation. The above six boundary conditions lead to the following linear equations in the frequency–wave-number domain,

$$\mathbf{MA} = \mathbf{B}, \tag{50}$$

where

$$\mathbf{A} = \{A_m, B_e, A_{pf}, A_{ps}, A_{sh}, A_{em}\}^T, \tag{51}$$

$$\mathbf{B} = \left\{ 0,0,0,0, \frac{i\omega\mu p_e}{4\pi^2} \times \left(1 - \frac{k^2}{k_{be}^2}\right) K_0(\eta_{be} r), \frac{i\omega\mu p_e}{4\pi^2} \eta_{be} K_1(\eta_{be} r) \right\}^T, \quad (52)$$

and the elements of **M** are shown in Appendix A.

D. The uncoupled method

In the above derivation the acoustic field and the EM field are coupled in the formation; the process of obtaining the coupled fields is complicated. It may be much more complicated, or even impossible, to formulate the coupled fields for more complex geometries or more complex source distributions. If the formation is assumed to be heterogeneous, it is difficult to get analytical expressions for the fields. So, in this subsection, we adopt a different method to simulate E-A logging without solving directly the coupled fields in the formation. We called this method the uncoupled method in order to distinguish it from the coupled method in the above study. We hope this uncoupled method will be a check to the coupled method in some way.

In E-A logging, the EM wave excited by the source induces the acoustic field in the porous formation and the converted acoustic field influences back on the EM field because of the electrokinetic effect. Nevertheless, if the reverse influence is weak enough, we can assume it is negligible. We will validate the feasibility of this assumption by comparison of the coupled and uncoupled waveforms in Sec. 3. When the influence is negligible, the second term on the right hand of Eq. (5) becomes zero; the EM field in the formation can be obtained separately by solving Maxwell's equations. According to the theory of electrodynamics, electric field **E** in the source-free formation must obey the following equations,

$$\nabla^2 \mathbf{E} + k_{em}^2 \mathbf{E} = 0, \quad (53)$$

$$\nabla \cdot \mathbf{E} = 0, \quad (54)$$

where

$$k_{em}^2 = \omega^2 \mu\varepsilon + i\omega\mu\sigma. \quad (55)$$

From Eqs. (53) and (54) and using Eq. (21), we obtain expressions for the EM field in the frequency domain,

$$E_z = \int_{-\infty}^{\infty} A_e \frac{\eta_{em}}{ik} K_0(\eta_{em} r) e^{ikz}\, dk, \quad (56)$$

$$E_r = \int_{-\infty}^{\infty} A_e K_1(\eta_{em} r) e^{ikz}\, dk, \quad (57)$$

$$H_\theta = \int_{-\infty}^{\infty} A_e \frac{1}{\omega\mu} \left(k - \frac{\eta_{em}^2}{k}\right) K_1(\eta_{em} r) e^{ikz}\, dk. \quad (58)$$

where the unknown coefficient A_e can be determined by the boundary conditions at the borehole wall. Recalling that the EM field is not coupled with the acoustic field in the borehole fluid because there is no electrokinetic effect in it, Eq. (35) remains valid for the EM field in the borehole, but the coefficient B_e in Eqs. (32)–(34) is different now. We can obtain B_e as well as A_e in Eqs. (56)–(58) by imposing the boundary conditions for the EM field at the borehole wall. These boundary conditions are expressed as a set of linear equations in Appendix B.

Upon knowing the EM field, we can determine the converted acoustic field. The acoustic field still satisfies Eqs. (11) and (12). Notice that the last term on the left side of Eq. (12) depends on the known electric field **E** and can be considered as the source of the acoustic field. If **E** becomes zero, Eq. (12) turns to

$$C \nabla \nabla \cdot \mathbf{u} + \omega^2 \rho_f \mathbf{u} + M \nabla \nabla \cdot \mathbf{w} + \omega^2 \bar{\rho} \mathbf{w} = 0. \quad (59)$$

Equations (11) and (59) are the homogeneous Biot equations for acoustic waves in porous medium and can be solved as in the paper by Rosenbaum (1974). Now we expound on how to find a set of particular solutions for Eqs. (11) and (12). Let $\mathbf{u}^0$ and $\mathbf{w}^0$ be the set of particular solutions that are related to the electric field **E** as

$$\mathbf{u}^0 = T_1 \mathbf{E}, \quad \mathbf{w}^0 = T_2 \mathbf{E}, \quad (60)$$

where the coefficients T_1 and T_2 are be to determined as follows.

According to Eq. (54), we have

$$\nabla \cdot \mathbf{u}^0 = 0, \quad \nabla \cdot \mathbf{w}^0 = 0. \quad (61)$$

By substituting Eqs. (60) and (61) into Eqs. (11) and (12) we get

$$G T_1 \nabla^2 \mathbf{E} + (\omega^2 \rho T_1 + \omega^2 \rho_f T_2) \mathbf{E} = 0, \quad (62)$$

$$(\omega^2 \rho_f T_1 + \omega^2 \bar{\rho} T_2 - i\omega\bar{\rho} L) \mathbf{E} = 0. \quad (63)$$

A comparison between Eq. (53) and (62) leads to

$$(\omega^2 \rho T_1 + \omega^2 \rho_f T_2)/(G T_1) = k_{em}^2. \quad (64)$$

And, from Eq. (63), we have

$$\omega^2 \rho_f T_1 + \omega^2 \bar{\rho} T_2 - i\omega\bar{\rho} L = 0, \quad (65)$$

for a nontrivial solution of **E**.

Solving simultaneously Eqs. (64) and (65), one obtains the coefficients T_1 and T_2:

$$T_1 = \frac{iL}{\omega} \left(\frac{G k_{em}^2}{\omega^2 \rho_f} - \frac{\rho}{\rho_f} + \frac{\rho_f}{\bar{\rho}} \right)^{-1}, \quad (66)$$

$$T_2 = \frac{i\omega\bar{\rho} L - \omega^2 \rho_f T_1}{\omega^2 \bar{\rho}}. \quad (67)$$

By this time we have a set of particular solutions. And the solution for the converted acoustic field in the formation can be obtained by superposing the solution of the homogenous equation and the set of particular solutions.

Similar to the coupled method, we can solve for the unknown coefficients in the expressions for the acoustic fields in the formation and in the borehole by imposing boundary conditions at the borehole wall. These conditions lead to a set of linear equations as is given in Appendix C. The expressions (41)–(43) for the acoustic field in the borehole remain valid for the uncoupled method as long as the

TABLE I. Input parameters for simulating E-A logging. The relationships between ϕ and K_b and G_b are assumed to obey the experimental results of Vernik (1994). ε_0 is the permittivity of vacuum.

Parameter	Property	Value
a	Borehole radius (m)	0.1
ϕ	Porosity (%)	20
κ_0	Static Darcy permeability (Darcy)	1
K_b	Frame bulk modulus (GPa)	14.39
G_b	Frame shear modulus (GPa)	13.99
K_s	Solid bulk modulus (GPa)	35.70
K_f	Pore fluid bulk modulus (GPa)	2.25
ρ_s	Solid density (Kg/m^3)	2650
ρ_f, ρ_b	Pore fluid density, borehole fluid density (Kg/m^3)	1000
ε_s	Solid permittivity	$4\varepsilon_0$
$\varepsilon_f, \varepsilon_b$	Pore fluid permittivity, borehole fluid permittivity	$80\varepsilon_0$
C_f, C_b	Pore fluid salinity, borehole fluid salinity (mol/L)	0.01
η	Pore fluid viscosity (Pa·s)	10^{-3}
V_{bm}	Acoustic velocity in borehole fluid (m/s)	1500
Q_{bm}	Quality factor in the borehole fluid	100
T	Temperature (K)	298
α_∞	Tortuosity	3

coefficient A_m is determined according to Appendix C.

III. NUMERICAL SIMULATIONS

To simulate the E-A logging response, we calculated the E-A pressure p as well as the three components of the EM field, i.e., radial and axial components of the electric field E_r and E_z, and circumferential magnetic field H_θ. Although, in real logging tools, an acoustic receiver can not be placed at the same point where an EM field is sensed, it is assumed in our calculation that all four quantities can be measured at any point in the borehole. We first calculate the four fields in the frequency domain expressed by Eqs. (28)–(30) and (32)–(35) in the coupled method or Eqs. (56)–(58) in the uncoupled method and Eq. (41), and then Fourier transform them to get the time-domain response. For example, p in the borehole is

$$p(t) = \frac{1}{2\pi}\int_{-\infty}^{+\infty} p(\omega) S_0(\omega) e^{-i\omega t}\, d\omega, \tag{68}$$

where $p(\omega)$ is the frequency-domain response obtained from Eq. (41), and $S_0(\omega)$ is the spectrum of the source pulse function $s_0(t)$,

$$s_0(t) = \begin{cases} \frac{1}{2}\left[1 + \cos\frac{2\pi}{T_c}\left(t - \frac{T_c}{2}\right)\right]\cos 2\pi f_0\left(t - \frac{T_c}{2}\right), & 0 \leqslant t \leqslant T_c \\ 0, & t < 0 \quad or \quad t > T_c \end{cases}, \tag{69}$$

where f_0 is the center frequency and T_c is the pulse width. In all of the numerical simulation examples below, we adopt an f_0 of 6 kHz and a T_c of 0.5 ms. The source intensity p_e of the electric dipole is assumed to be 1 A·m. The formation of our model is assumed to be consolidated sandstone, and the parameter relationships between the porosity ϕ and the frame moduli K_b and G_b are assumed to obey the experimental results of Vernik (1994). The input parameters of the model for simulating E-A logging are listed in Table I unless explicitly stated elsewhere.

We performed the simulations and obtained the waveforms by the two different methods introduced above. Then we calculated the difference waveforms when the same input parameters are used in the two methods and found the largest relative difference in amplitude is in the order of 10^{-4} for all examples in the paper. Such a small relative difference cannot be seen in the plots of waveforms. We think the difference partially results from the truncation error due to limited computer digits, and partially comes from the difference in conversion mechanism (the reverse influence is ignored in the uncoupled method). This conclusion of remarkably small difference is important because of lack of reachable experimental data to be used as a reference, and makes us confident in our calculations. It also proved that the uncoupled method in which the acoustic field is calculated after the EM field being evaluated separately is feasible and accurate. Thus we do not need to point out which waveforms are simulated by which method in the following examples.

Now let us study the properties of the converted acoustic field during E-A logging. Figure 1 shows the full waveforms of E-A pressure p on the borehole axis, when the distance to the source z varies from 3.0 to 4.5 m. Obviously, there are

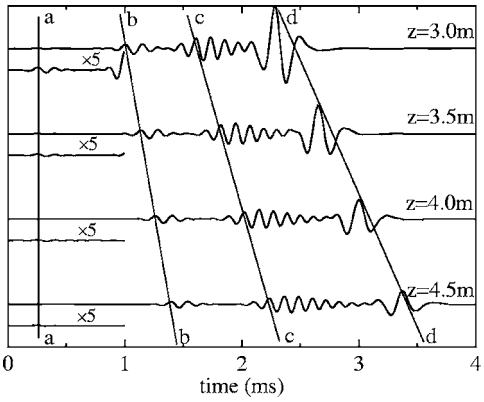

FIG. 1. Transient full waveforms of E-A pressure p on the borehole axis when the distance to the source z varies from 3 to 4.5 m. The waveforms are scaled to the wave magnitude at $z=3$ m. The waveforms in the first millisecond are magnified by five times.

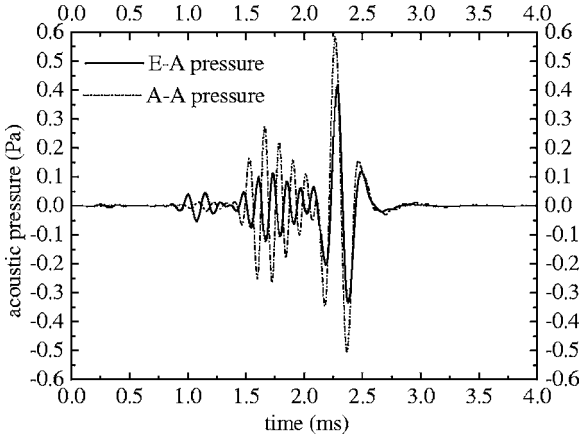

FIG. 2. Comparison between the waveforms of E-A pressure p and that in A-A logging. Both of the waveforms are calculated on the borehole axis at $z=3$ m.

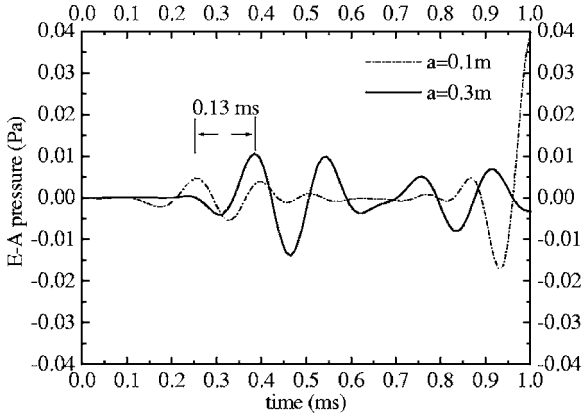

FIG. 3. Waveforms of E-A pressure p on the borehole axis at $z=3$ m when the borehole radii are 0.1 and 0.3 m. Only waves in the first millisecond are shown. The earliest arrival delays about 0.13 ms when the borehole radius changes from 0.1 to 0.3 m.

three different wave groups in the waveforms (shown by lines b-b, c-c, and d-d, respectively, in Fig. 1). In Fig. 2 we compare the waveform of E-A pressure p and that in acoustic-to-acoustic (A-A) logging. The waveform in A-A logging is calculated using Biot's theory, as done by Rosenbaum (1974). An acoustic point source as described in Tsang and Rader (1979) is used in the A-A logging simulation, with the peak pressure being 100Pa at a location of 0.01 m away from the point source. The same source function is used as that in E-A logging, with $f_0=6$ kHz, $T_c=0.5$ ms. Other required input parameters are the same as those in E-A logging and are given in Table I. It is seen that the three wave groups in the E-A logging waveform have the same wave velocities as those in A-A logging. From previous research on A-A logging, we conclude that the three wave groups are, in order of arrival time, the compressional wave group, the shear and pseudo-Rayleigh wave group, and the Stoneley wave group. These wave groups are originated at the borehole wall through conversion of EM energy to mechanical energy. Once generated, they propagate independently of the electric field.

When we magnify by five times the first millisecond of the waveforms in Fig. 1, we see a wave group (showed by line a-a in Fig. 1) that arrives earlier than the compressional wave group and reaches the four different receivers at almost the same time. In Fig. 3 we compare the first millisecond waveforms of E-A pressure p in boreholes with different radii. When the radius changes from 0.1 to 0.3 m, the earliest wave group delays 0.13 ms, which is the time for an acoustic wave in the borehole fluid to travel 0.2 m. We judge from this phenomenon that this wave group is a real physical signal rather than a spurious signal resulting from calculation. A further comparison is shown in Fig. 4 between the waveform of the electric field E_z and that of the E-A pressure p. The earliest acoustic disturbance, i.e., the wave group that arrives before the compressional wave, seems to accompany the electric field and to possess an apparent phase velocity of the EM wave in the formation. This phenomenon is consistent with an earlier theoretical prediction by Pride and Haartsen (1996). This wave group is induced by the conversion of the EM wave on the borehole wall at different depths and reflected back to the borehole fluid, which is named as an EM-accompanying acoustic group.

Now we investigate the effect of formation parameters on E-A logging. We focus our study on the effects of permeability and porosity in this paper. Shown in Fig. 5 are the waveforms of E-A pressure p for the permeability κ_0 being 0.01 and 10 Darcy. The amplitude of E-A pressure changes with permeability. Among all the wave groups, the E-A Stoneley wave group is the most sensitive to permeability. The E-A Stoneley wave amplitude decreases with the increase of permeability, which is similar to the case in A-A logging. From Figs. 5(a) and 5(b), the E-A Stoneley wave amplitude decreases 96.8% and 99.1% at the locations $z=3$ m and $z=4.5$ m, respectively, when permeability increases from 0.01 to 10 Darcy. The sensitivity to permeability increases with the distance to the source, since the acoustic propagation attenuation increases with permeability as well as the distance to the source.

Similar to the way of considering the effects of permeability above, we found that the E-A Stoneley wave group is also the most sensitive to porosity. In order to reveal possible relationships between the E-A Stoneley wave amplitude and

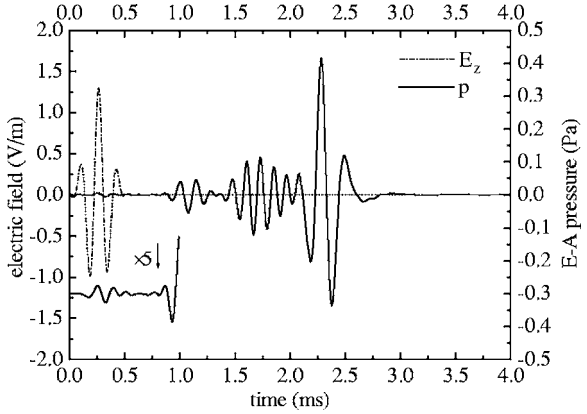

FIG. 4. Waveforms of E-A pressure p and electric field E_z on the borehole axis at $z=3$ m. Also shown in the figure is the front part of the waveform of E-A pressure p, which is magnified by five times for the comparison with the waveform of electric field E_z.

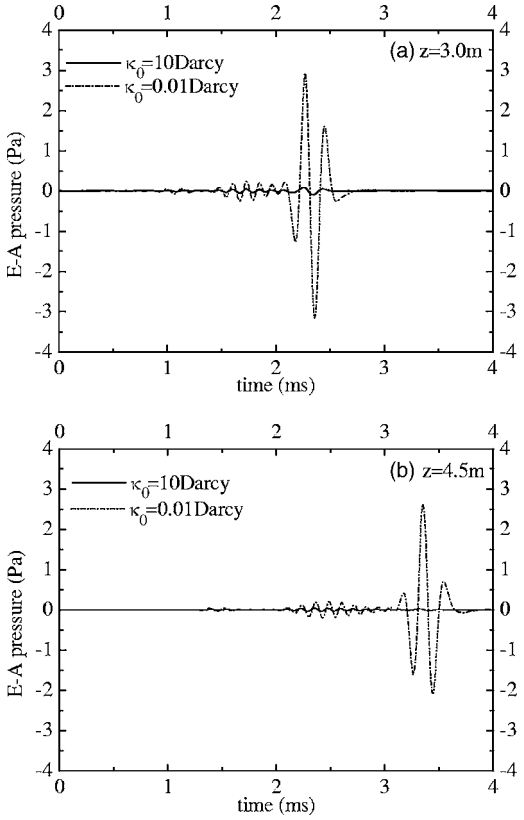

FIG. 5. Waveforms of E-A pressure p for permeabilities κ_0 of 10 and 0.01 Darcy. (a) Measured on the borehole axis at $z=3$ m. (b) Measured on the borehole axis at $z=4.5$ m.

permeability and porosity, and to discuss some different characteristics between E-A logging and A-A logging, calculations are performed under a series of combinations of permeability and porosity for E-A logging and A-A logging. The results are listed in Table II. To show the variations clearly, we plotted the results in Figs. 6 and 7 for E-A logging and A-A logging, respectively, according to the data in Table II. As shown in Fig. 6, when permeability is much lower than 1 Darcy, the E-A Stoneley wave amplitude is highly dependent on porosity as well as permeability: the higher the porosity, the larger the amplitude, and the higher the permeability, the smaller the amplitude. The effect of porosity on E-A Stoneley wave amplitude is different from that in A-A logging (see Fig. 7). This is not outside our expectation because two mechanisms together control the amplitude change of the E-A Stoneley wave. One is the E-A conversion ratio determined by the electrokinetic coupling coefficient L, and the other is the attenuation of the converted wave during its propagation in the porous medium. While the second mechanism is shared by A-A logging, the first mechanism belongs to E-A logging only. The A-A Stoneley wave amplitude decreases monotonically when porosity increases, because waves in a high porosity formation usually attenuate faster. In E-A logging, however, due to a larger L at a higher porosity, which is described by Eq. (10), and which means a stronger coupling between EM field and acoustic field, E-A pressure may increase with porosity. When permeability reaches 10 Darcy, the amplitude decreases with the increasing porosity (see Table II), revealing that the attenuation mechanism dominates amplitude variation. Thus there is a critical permeability where the amplitude of the Stoneley wave is invariant with porosity. From the data in Table II, it is calculated that E-A Stoneley wave amplitude decreases 68.6%, 79.5%, and 83.0% for porosity being 10%, 20%, and 25%, respectively, when permeability increases from 1 to 10 Darcy. But the A-A Stoneley wave amplitude de-

TABLE II. Stoneley wave amplitudes obtained from E-A logging and A-A logging with different porosities and permeabilities.

Porosity (%)	Permeability (Darcy)	Amplitude of Stoneley wave (Pa)	
		E-A logging	A-A logging
10	0.01	1.519	3.970
10	0.1	1.142	2.974
10	1.0	0.354	1.361
10	10	0.111	1.205
20	0.01	2.931	3.671
20	0.1	2.033	2.523
20	1.0	0.416	0.585
20	10	0.092	0.387
25	0.01	3.530	3.509
25	0.1	2.373	2.293
25	1.0	0.399	0.428
25	10	0.068	0.248

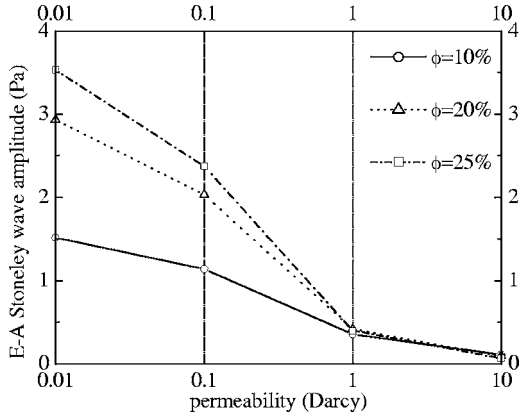

FIG. 6. Showing the amplitude variation of the E-A Stoneley wave with different porosities and permeabilities, according to the data in Table II.

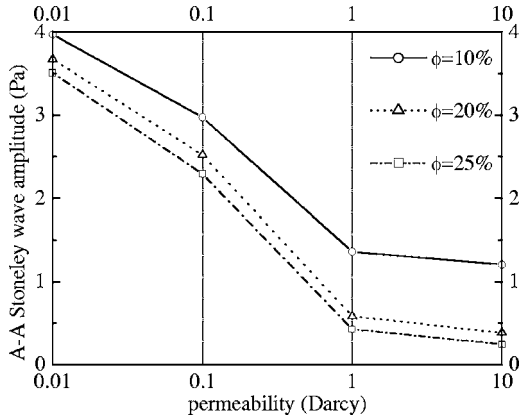

FIG. 7. Showing the amplitude variation of the A-A Stoneley wave with different porosities and permeabilities, according to the data in Table II.

creases 11.5%, 33.8%, and 42.0%, respectively, in the same situations. This reveals that E-A Stoneley wave amplitude drops more sharply in the high permeability range than that in conventional A-A logging. The A-A Stoneley wave amplitude is sensitive to porosity rather than permeability (see Fig. 7) in the high permeability range. In the paper by Wu *et al.* (1995), the error is large in estimating permeability from Stoneley wave attenuation when permeability is larger than 2 Darcy, because of the small change with permeability in the amplitude of the Stoneley wave in the high permeability range. The E-A Stoneley wave can be used instead for the inversion of permeability in highly permeable formations.

IV. CONCLUSIONS

A coupled method and an uncoupled method are put forward for simulating the axisymmetric fields of E-A logging in a fluid-saturated porous medium. A vertical electric dipole on the borehole axis is used as the exciting source. In the coupled method, the acoustic and EM fields in the formation are formulated by using Pride's governing equations. In the uncoupled method, the EM field is obtained by solving Maxwell's equations; the acoustic wave field is then obtained by solving linear inhomogeneous Biot equations, with the source term, due to the electrokinetic effect, originating from the EM disturbances. This uncoupled method is possible because the influence from the converted acoustic field on the EM field is negligible.

The transient full waveforms for the electric field and the converted acoustic field in the borehole are simulated by the two methods. In order to compare the waveforms obtained by the two methods, the difference waveforms are calculated when the same input parameters are used. It is found that the largest relative difference in amplitude is in the order of 10^{-4} for all examples in this paper, so that cannot be seen in the plots of waveforms. It proved that the uncoupled method is correct and feasible. The idea behind the uncoupled method can be extended to evaluate E-A conversion response in more complex geometric situations in which the analytical solution is unobtainable. For example, if the fluid-saturated formation outside the borehole is stratified horizontally, there will be no analytical solution to either the EM field or the acoustic field. But we can solve for the EM field first by a well established finite-element or finite-difference method, and then solve for the inhomogeneous acoustic field by the same numerical technique.

The full waveform of the converted acoustic field in E-A logging contains four wave groups: EM-accompanying wave group, compressional wave group, shear and pseudo-Rayleigh wave group, and Stoneley wave group. The EM-accompanying wave group accompanies the EM field and has an apparent phase velocity of the EM wave, but is a mechanical disturbance in itself. The other three wave groups can propagate independently of the EM field and are generated when the EM wave emitted by the electric dipole travels across the borehole wall.

The amplitude of E-A Stoneley wave changes with permeability and porosity. It decreases with permeability, similar to conventional A-A logging. It decreases with porosity when permeability is very high (several Darcies or higher), but increases with porosity in the common sediment rock permeability range. This is because the amplitude of the E-A Stoneley wave is indirectly affected by porosity in two different ways. It is affected by porosity through the electrokinetic coupling coefficient L as well as through propagation attenuation. The coefficient L increases with porosity, while propagation attenuation increases with porosity. When permeability is small, the variation of the E-A Stoneley wave amplitude is dominated by L, resulting in the increase of the E-A Stoneley wave amplitude with porosity. Nevertheless, when permeability is high enough, the attenuation mechanism dominates, and the E-A Stoneley wave amplitude decreases with increasing porosity. There is a critical permeability where the E-A Stoneley wave amplitude does not change with porosity. When permeability reaches or exceeds 1 Darcy, the sensitivity of the E-A Stoneley wave amplitude to permeability is higher than that in A-A logging.

ACKNOWLEDGMENTS

The first author would like to express his gratitude to Professor Kexie Wang at Jilin University of China for his help on analysis of related wave phenomena, and to Dr. Zhenya Zhu at Massachusetts Institute of Technology for his lectures on seismoelectric experiments. This work is supported by the National Natural Science Foundation of China (Grant No. 10272038). This work was completed while the first author was visiting the Wave Physics Laboratory at Stanford University.

APPENDIX A: EXPRESSIONS OF THE ELEMENTS OF *M* IN EQ. (50)

$$m_{11} = \eta_{bm} I_1(\eta_{bm} a)/\pi,$$

$$m_{21} = m_{31} = \rho_b \omega^2 I_0(\eta_{bm} a)/\pi,$$

$$m_{41} = m_{51} = m_{61} = m_{12} = m_{22} = m_{32} = 0,$$

$$m_{42} = m_{63} = m_{64} = m_{25} = m_{26} = 0,$$

$$m_{13} = \eta_{pf}(1 + \alpha_{pf}) K_1(\eta_{pf} a),$$

$$m_{14} = \eta_{ps}(1 + \alpha_{ps}) K_1(\eta_{ps} a),$$

$$m_{15} = ik(1 + \alpha_{sh}) K_1(\eta_{sh} a),$$

$$m_{16} = ik(1 + \alpha_{em}) K_1(\eta_{em} a),$$

$$m_{23} = -k_{pf}^2 (C + M\alpha_{pf}) K_0(\eta_{pf} a),$$

$$m_{24} = -k_{ps}^2 (C + M\alpha_{ps}) K_0(\eta_{ps} a),$$

$$m_{33} = \frac{2G\eta_{pf} K_1(\eta_{pf} a)}{a} + [(2G - H - C\alpha_{pf}) k_{pf}^2 + 2G\eta_{pf}^2] K_0(\eta_{pf} a),$$

$$m_{34} = \frac{2G\eta_{ps}K_1(\eta_{ps}a)}{a} + [(2G - H - C\alpha)k_{ps}^2 + 2G\eta_{ps}^2]K_0(\eta_{ps}a),$$

$$m_{35} = 2ikG[\eta_{sh}K_0(\eta_{sh}a) + K_1(\eta_{sh}a)/a],$$

$$m_{36} = 2ikG[\eta_{em}K_0(\eta_{em}a) + K_1(\eta_{em}a)/a],$$

$$m_{43} = -2ik\eta_{pf}K_1(\eta_{pf}a),$$

$$m_{44} = -2ik\eta_{ps}K_1(\eta_{ps}a),$$

$$m_{45} = (k^2 + \eta_{sh}^2)K_1(\eta_{sh}a),$$

$$m_{46} = (k^2 + \eta_{em}^2)K_1(\eta_{em}a),$$

$$m_{52} = \eta_{be}I_0(\eta_{be}a)/ik,$$

$$m_{53} = ik\beta_{pf}K_0(\eta_{pf}a),$$

$$m_{54} = ik\beta_{ps}K_0(\eta_{ps}a),$$

$$m_{55} = -\beta_{sh}\eta_{sh}K_0(\eta_{sh}a),$$

$$m_{56} = -\beta_{em}\eta_{em}K_0(\eta_{em}a),$$

$$m_{62} = i(\eta_{be}^2/k - k)I_1(\eta_{be}a),$$

$$m_{65} = \beta_{sh}k_{sh}^2K_1(\eta_{sh}a). \quad \text{(A1)}$$

$$m_{66} = \beta_{em}k_{em}^2K_1(\eta_{em}a). \quad \text{(A1)}$$

APPENDIX B: EXPRESSIONS OF THE LINEAR EQUATIONS FOR EM FIELD IN THE UNCOUPLED METHOD

To determine the unknown coefficients A_e in Eqs. (56)–(58) and B_e in Eqs. (32)–(34), we impose the boundary conditions at the borehole wall, i.e., continuity of the axial component of the electric field and continuity of the circumferential component of the magnetic field. These conditions lead to the following linear equations:

$$\begin{bmatrix} m_{11}m_{12} \\ m_{21}m_{22} \end{bmatrix} \cdot \begin{bmatrix} A_e \\ B_e \end{bmatrix} = \begin{bmatrix} y_1 \\ y_2 \end{bmatrix}, \quad \text{(B1)}$$

where

$$m_{11} = \frac{\eta_{em}}{ik}K_0(\eta_{em}a),$$

$$m_{12} = \frac{\eta_{be}}{ik}I_0(\eta_{be}a),$$

$$m_{21} = \frac{1}{\omega\mu}\left(k - \frac{\eta_{em}^2}{k}\right)K_1(\eta_{em}a),$$

$$m_{22} = -\frac{1}{\omega\mu}\left(k - \frac{\eta_{be}^2}{k}\right)I_1(\eta_{be}a),$$

$$y_1 = \frac{\mu p_e}{4\pi^2}i\omega\left(1 - \frac{k^2}{k_{be}^2}\right)K_0(\eta_{be}a),$$

$$y_2 = \frac{p_e}{4\pi^2}\eta_{be}K_1(\eta_{be}a). \quad \text{(B2)}$$

APPENDIX C: EXPRESSIONS OF THE LINEAR EQUATIONS FOR ACOUSTIC FIELD IN THE UNCOUPLED METHOD

Here we establish the linear equations to solve the unknown coefficients in the expressions for the acoustic fields in the formation and in the borehole in the uncoupled method by employing the acoustic field boundary conditions at the borehole wall. These boundary conditions are the same as Eqs. (44)–(47). The linear equations are expressed below in the frequency-wavenumber domain:

$$\mathbf{MA} = \mathbf{B}, \quad \text{(C1)}$$

where

$$\mathbf{A} = \{A_m, A_{pf}, A_{ps}, A_{sh}\}^T, \quad \text{(C2)}$$

$$\mathbf{B} = \{b_1, b_2, b_3, b_4\}^T, \quad \text{(C3)}$$

and the elements of $\mathbf{M}$ and $\mathbf{B}$ are given by

$$m_{11} = \frac{\eta_{bm}I_1(\eta_{bm}a)}{\rho_b\omega^2},$$

$$m_{21} = m_{31} = I_0(\eta_{bm}a),$$

$$m_{12} = \eta_{pf}(1 + \alpha_{pf})K_1(\eta_{pf}a),$$

$$m_{13} = \eta_{ps}(1 + \alpha_{ps})K_1(\eta_{ps}a),$$

$$m_{14} = ik(1 + \alpha_{sh})K_1(\eta_{sh}a),$$

$$m_{41} = m_{24} = 0,$$

$$m_{22} = -k_{pf}^2(C + M\alpha_{pf})K_0(\eta_{pf}a),$$

$$m_{23} = -k_{ps}^2(C + M\alpha_{ps})K_0(\eta_{ps}a),$$

$$m_{32} = 2G\eta_{pf}\frac{K_1(\eta_{pf}a)}{a} + [2Gk^2 - (H + \alpha_{pf}C)k_{pf}^2]K_0(\eta_{pf}a),$$

$$m_{33} = 2G\eta_{ps}\frac{K_1(\eta_{ps}a)}{a} + [2Gk^2 - (H + \alpha_{ps}C)k_{ps}^2]K_0(\eta_{ps}a),$$

$$m_{34} = 2Gik\left[\eta_sK_0(\eta_{sh}a) + \frac{K_1(\eta_{sh}a)}{a}\right],$$

$$m_{42} = -2ik\eta_{pf}K_1(\eta_{pf}a),$$

$$m_{43} = -2ik\eta_{ps}K_1(\eta_{ps}a),$$

$$m_{44} = (k^2 + \eta_{sh}^2)K_1(\eta_{sh}a),$$

$$b_1 = (T_1 + T_2)A_e K_1(\eta_{em} a),$$

$$b_2 = 0,$$

$$b_3 = 2GT_1 A_e \left(\eta_{em} K_0(\eta_{em} a) + \frac{1}{a} K_1(\eta_{em} a) \right),$$

$$b_4 = \frac{k^2 + \eta_{em}^2}{ik} T_1 A_e K_1(\eta_{em} a). \quad \text{(C4)}$$

Biot, M. A. (**1956**). "Theory of propagation of elastic waves in a fluid-saturated porous solid. I. low-frequency range," J. Acoust. Soc. Am. **28**, 168–178.

Biot, M. A. (**1962**). "Mechanics of deformation and acoustic propagation in porous media," J. Appl. Phys. **33**, 1482–1498.

Broding, R., Buchanan, S., and Hearn, D. (**1963**). "Field experiments on the electroseismic effect," IEEE Trans. Geosci. Electron. **GE-1**, 23–31.

Butler, K. E., Russel, R. D., Kepic, A. W., and Maxwell, M. (**1996**). "Measurement of the seismoelectric response from a shallow boundary," Geophysics **61**, 1769–1778.

Frenkel, J. (**1944**). "On the theory of seismic and seismoelectric phenomena in a moist soil," (in Russian), J. Phys. (Moscow) **8**(4), 230–241.

Guru, B. S., and Hiziroğlu, H. R. (**2004**). *Electromagnetic Field Theory Fundamentals*, 2nd ed. (Cambridge U.P., London), p. 553.

Haartsen, M. W., and Pride, S. R. (**1997**). "Electroseismic waves from point sources in layered media," J. Geophys. Res. **102**(B11), 24745–24769.

Hu, H. (**2000**). Ph.D. thesis, Jilin University, China, (in Chinese).

Hu, H., and Liu, J. (**2002**). "Simulation of the converted electric field during acoustoelectric logging," 72nd Annual International Meeting, Soc. Exploration Geophysics, Expanded Abstracts, Vol. **21**, pp. 348–351.

Ivanov, A. G. (**1940**). "The electroseismic effect of the second kind," Bull. Acad. Sci. USSR, Geophys. Ser. **5**, 699–727 (in Russian).

Johnson, D. L., Koplik, J., and Dashen, R. (**1987**). "Theory of dynamic permeability and tortuosity in fluid-saturated porous media," J. Fluid Mech. **176**, 379–402.

Long, L. T., and Rivers, W. K. (**1975**). "Field measurement of the electroseismic response," Geophysics **40**, 233–425.

Martner, S. T., and Sparks, N. R. (**1959**). "The electroseismic effect," Geophysics **24**, 297–308.

Mikhailov, O. V., Haartsen, M. W., and Toksöz, M. N. (**1997**). "Electroseimic investigation of the shallow subsurface: Field measurements and numerical modeling," Geophysics **62**, 97–105.

Neev, J., and Yeatts, F. R. (**1989**). "Electrokinetic effects in fluid-saturated poroelastic media," Phys. Rev. B **40**, 9135–9141.

Pride, S. R., and Morgan, F. (**1991**). "Electrokinetic dissipation induced by seismic waves," Geophysics **56**, 914–925.

Pride, S. R. (**1994**). "Governing equations for the coupled electromagnetics and acoustics of porous media," Phys. Rev. B **50**, 15678–15696.

Pride, S. R., and Haartsen, M. W. (**1996**). "Electroseismic wave properties," J. Acoust. Soc. Am. **100**, 1301–1315.

Rosenbaum, J. H. (**1974**). "Synthetic microseismograms: logging in porous formations," Geophysics **39**, 14–32.

Thompson, A. H. (**2005**). "Electromagnetic-to-seismic conversion: successful developments suggest viable applications in exploration and production," 75th Annual International Meeting, Soc. Exploration Geophysics, Expanded Abstracts, Vol. **24**, pp. 554–556.

Thompson, A. H., Hornbostel, S., Burns, J., Murray, T., Raschke, R., Wride, J., McCammon, P., Sumner, J., Haake, G., Bixby, M., Ross, W., White, B., Zhou, M., and Peczak, P. (**2005**). "Field tests of electroseismic hydrocarbon detection," 75th Annual International Meeting, Soc. Exploration Geophysics, Expanded Abstracts, Vol. **24**, pp. 565–568.

Thompson, A. H., and Gist, G. A. (**1993**). "Geophysical applications of electrokinetic conversion," The Leading Edge **12**, 1169–1173.

Tsang, L., and Rader, D. (**1979**). "Numerical evaluation of the transient acoustic waveform due to a point source in a fluid-filled borehold," Geophysics **44**, 1706–1720.

Vernik, L. (**1994**). "Predicting lithology and transport properties from acoustic velocities based on petrophysical classification of siliclastics," Geophysics **59**, 420–427.

Wu, X., Wang, K., Guo, L., Yu, S., and Dong, Q. (**1995**). "Inversion of permeability from the full waveform acoustic logging data," Acta Geophys. Sin. Suppl. I **38**, 224–231 (in Chinese).

Zhu, Z., Haartsen, M. W., and Toksöz, M. N. (**1999**). "Experimental studies of electrokinetic conversions in fluid-saturated borehole models," Geophysics **64**, 1349–1356.

Zhu, Z., and Toksöz, M. N. (**2003**). "Crosshole seismoelectric measurements in borehole models," Geophysics **68**, 1519–1524.

Zhu, Z., and Toksöz, M. N. (**2005**). "Seismoelectric and seismomagnetic measurements in fractured borehole models," Geophysics **70**, F45–F51.